THE JOURNAL OF PHYSICAL CHEMISTRY Letters

pubs.acs.org/JPCL Letter

# Quantum Effects Dominating the Interatomic Coulombic Decay of an Extreme System

Anael Ben-Asher, Arie Landau, Lorenz S. Cederbaum, and Nimrod Moiseyev*

Cite This: J. Phys. Chem. Lett. 2020, 11, 6600−6605 Read Online

ACCESS | Metrics & More | Article Recommendations

**ABSTRACT:** LiHe is an extreme open-shell system. It is among the weakest bound systems known, and its mean interatomic distance extends dramatically into the classical forbidden region. Upon 1s → 2p excitation of He, interatomic Coulombic decay (ICD) takes place in which the electronically excited helium atom relaxes and transfers its excess energy to ionize the neighboring lithium atom. A substantial part of the decay is found to be to the dissociation continuum producing $Li^+$ and He atoms. The distribution of the kinetic energy released by the ICD products is found to be highly oscillatory. Its analysis reveals that quantum phase shifts between the decaying states and the dissociating final states are controlling this ICD reaction. The semiclassical reflection principle, which commonly explains ICD reactions, fails. The process is expected to be amenable to experiment.

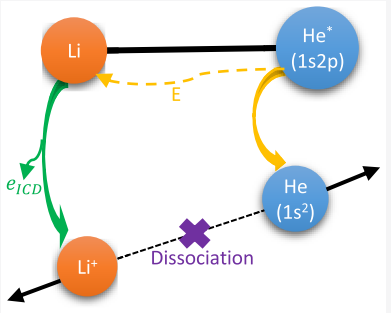


Downloaded via UNIV HEIDELBERG on November 3, 2020 at 11:02:01 (UTC).
See https://pubs.acs.org/sharingguidelines for options on how to legitimately share published articles.

Lithium helium dimer is a fascinating open-shell system which has the potential to exhibit interesting quantum phenomena. It was first detected only in 2013[1] because it is a very weakly bound system with a binding energy of 1.5 mK for $^6$LiHe and 5.6 mK for $^7$LiHe.[2] Moreover, it is an extremely extended system; the mean separation between the two atoms is 48.53 Å for $^6$LiHe and 28.15 Å for $^7$LiHe.[2] Note that the outer classical turning point of their sole bound vibrational state is about 17 Å;[3] thus, LiHe is a *quantum halo* system,[4] i.e., a system in which the nuclei spend most of the time in the classically forbidden region. In this Letter, we aim to investigate the possibility of an interatomic Coulombic decay (ICD) process in LiHe. ICD is an ultralong range energy-transfer process, in which the energy emitted by the relaxation of a species (atom, molecule, or ion) is transferred to its neighbor and ionizes it.[5]

ICD was extensively studied theoretically and experimentally in various systems, including atomic and molecular dimers and larger clusters (see, for instance, refs 6−14). The potential importance of ICD in biologically relevant systems embedded in, for example, aqueous environment and in radiation damage has also been discussed.[8,15−18] An ICD investigation of another extremely weakly bound Van der Waals system, the helium dimer,[19,20] is of particular relevance to our present study. $He_2$ was detected only in 1993, although its existence raised interest decades before.[21] In this extreme quantum system, the mean separation of the two helium atoms is 52 Å,[22] although the outer classical turning point of the ground vibrational state is 14 Å.[3] As an extreme quantum system, the two helium atoms can exchange energy over large distances of more than 45 times their atomic radius during the ICD process as demonstrated experimentally and theoretically in ref 20. Notably, the ICD process occurs in $He_2$ after simultaneous ionization and excitation of one helium atom within the dimer. The ionized and excited helium relaxes into $He^+(1s)$ by transferring its excess energy to the ionization of the neutral helium into a second $He^+(1s)$ which results in an emitted ICD electron. Thus, the final state consists of two repelling $He^+$ ions undergoing a Coulombic explosion. The distribution of the kinetic energy released (KER) by the two helium ions after the ICD process reflects the wave function of the decaying state in accord with the semiclasical reflection principle.[23,24] Within the reflection principle, the vibrational wave function of the decaying state is projected onto the final potential energy curve, determining a one-to-one relationship between the internuclear distance and the KER spectrum. As was shown in ref 20 for the helium dimer, the projected wave function must be weighted by the distance-dependent ICD rate because of the extreme extent of this dimer. This extended semiclassical reflection principle predicts successfully the KER spectrum for ICD in $He_2$.[20]

The ICD process within LiHe is complementary to the case of the helium dimer. Unlike $He_2$, LiHe has one additional electron which makes it an open-shell dimer, and the electronic structure calculations of which become more challenging.[25] More relevant are the differences in the process itself. In the

Received: June 26, 2020
Accepted: July 24, 2020
Published: July 24, 2020

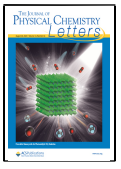

ACS Publications © 2020 American Chemical Society



https://dx.doi.org/10.1021/acs.jpclett.0c01974
J. Phys. Chem. Lett. 2020, 11, 6600−6605

$He_2$ case, ICD arises because of simultaneous excitation and ionization, whereas in the LiHe case, ICD is achieved solely upon excitation. Thus, the final states of the ICD process contain both the dissociative $Li^+$ and He as well as the bound dimer $Li^+$−He. This contrasts with the helium dimer example which undergoes Coulombic explosion. Consequently, studying ICD within LiHe presents the opportunity to investigate the decay into the bound vibrational states of $Li^+$−He, in addition to its dissociative states. Importantly, the semiclassical reflection principle, which explains the ICD process in the helium dimer as discussed above, fails in the LiHe case. Instead, we demonstrate that quantum phase shift effects determine the shape of the KER spectrum of ICD in LiHe.

The decaying state during the ICD process of LiHe dimer is associated with an excitation of the helium atom. The optically allowed transition of helium in its ground state is into its 1s2p $^1$P state, in which the stored energy, 21.22 eV, is sufficient to ionize the Li atom whose ionization energy is 5.39 eV. The resulting excited degenerate electronic state of the atom splits into $^2\Sigma$ and $^2\Pi$ states of the dimer, corresponding to the orientation of the 2p orbital of helium with respect to the interatomic axis. Notice that recently a related process was observed: ICD within helium nanodroplets doped with Li atom. In this case, the ICD occurs out of the $^1$S state of helium because this setup allows for ultrafast internal relaxation of the helium atom from its $^1$P state to its $^1$S state.[26] In contrast, in the LiHe dimer case this internal relaxation does not take place, and therefore, the $^1$S state of helium is not involved. Therefore, in the following, we investigate the above-mentioned $^2\Sigma$ and $^2\Pi$ states of LiHe dimer. These states have a finite lifetime and decay into the ionized complex, $Li^+$−He, and its dissociative states.

The $^2\Sigma$ and $^2\Pi$ metastable (resonance) states can be described by complex potential energy curves (CPECs).[27] The CPECs of the $^2\Sigma$ and $^2\Pi$ states were recently calculated[25] by the resonance via Padé (RVP) approach[28,29] based on the accurate equation-of-motion coupled-cluster (EOM-CC) method[30] and stabilization graphs.[31,32] The real part of the CPECs corresponds to their position energy (middle panel of Figure 1), and the imaginary part corresponds to their decay rate (top panel of Figure 1) as a function of the internuclear distance R. The *ab initio* $^2\Sigma$ and $^2\Pi$ decay rates have been extrapolated to have the general behavior of ICD rates at large interatomic distances, where $\Gamma(R)$ is proportional to $\frac{1}{R^6}$.[25,33] This behavior characterizes a long-range decay process compared to other decay processes in which the rate decays exponentially.[34,35] The real part of the $^2\Sigma$ and $^2\Pi$ CPECs exhibits potential wells which are deep enough (with a 4375 and 3054 K well depth, respectively) to support 20 and 27 vibrational states, respectively. In contrast, the cation's potential (lower panel of Figure 1), calculated[25] by EOM-CC, has a shallower well (its depth is 1017 K) and supports only 8 vibrational states. Importantly, its minimum is at a much smaller interatomic distance (1.9 Å) than the minima of $^2\Sigma$ and $^2\Pi$ potentials (3.4 Å). We note that the potential energy of the electronic ground state of the neutral dimer supports only a single vibrational state.

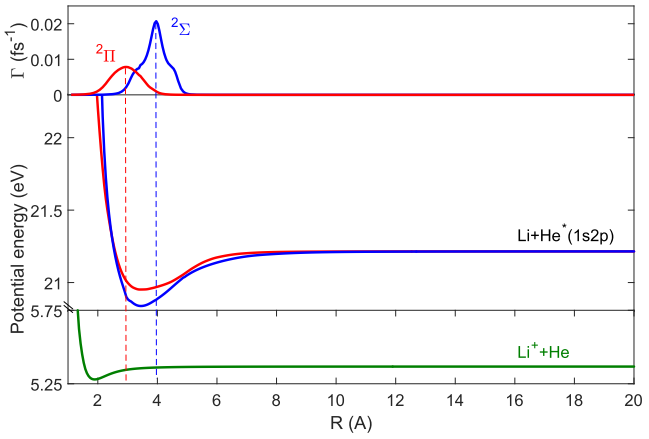


**Figure 1.** ICD rates of the $^2\Sigma$ and $^2\Pi$ decaying states of Li−He* (top panel). Potential curves of the decaying states $^2\Sigma$ and $^2\Pi$ (middle panel). Potential curve of the cationic product of the ICD, $Li^+$−He (lower panel). The potential energies are presented relative to the Li−He ground-state energy at the asymptote.

The electronic $^2\Sigma$ and $^2\Pi$ decay rates as a function of the nuclear separation determine the region in which the ICD reaction takes place. From Figure 1, we can see that decaying from the $^2\Sigma$ and from the $^2\Pi$ states occurs mostly in the region in which the potential of the cation is slightly attractive and is almost flat. Therefore, according to the semiclassical reflection principle, we expect that most of the ICD products are bound states of the cation, while the KER spectra contain only a broad peak around zero kinetic energy. However, the KER spectra (Figure 2) show a completely different behavior. The

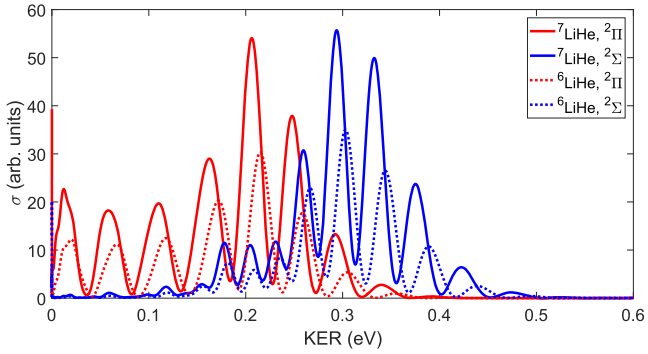


**Figure 2.** Distribution of kinetic energy released (KER) by the He and $Li^+$ after ICD, calculated using eq 1. The legend indicates the symmetry of the metastable electronic state participating in the ICD process and the involved isotope of Li.

KER spectra were computed by performing quantum nuclear dynamics on the CPECs.[36] As seen in Figure 2, these spectra exhibit a prominent oscillatory behavior giving rise to numerous peaks. Note that the range of the LiHe KER (0−0.5 eV) is very narrow relative to that in the $He_2$ case, in which the KER spectra spread up to 10 eV.[19,20] Although the semiclassical reflection principle also predicts very low KER for ICD in LiHe (but actually lower than the 0.5 eV), it fails in explaining the oscillatory behavior, i.e., the appearance of the peaks in the KER spectra.

In addition, the quantum dynamics on the CPECs predicts that the bound states of the cation constitute only a relatively small fraction of the ICD products of LiHe (see Table 1). This is contrary to the prediction of the semiclassical reflection principle. The decay of the $^2\Sigma$ state yields only 0.25% bound $Li^+$−He states and less than 12% for the $^2\Pi$ state (Table. 1). Note that the semiclassical reflection principle indeed predicts more bound products from $^2\Pi$ than from $^2\Sigma$. The reason is


https://dx.doi.org/10.1021/acs.jpclett.0c01974
J. Phys. Chem. Lett. 2020, 11, 6600−6605

**Table 1. Fraction of Bound Cationic States ($Li^+$−He) and of Dissociative Products ($Li^+$ and He) Populated by the ICD Reaction in Li−He*[a]**

| decaying state | bound states (%) | dissociative states(%) |
|---|---|---|
| $^6$LiHe, $^2\Sigma$ | 0.25 | 99.75 |
| $^6$LiHe, $^2\Pi$ | 11.83 | 88.17 |
| $^7$LiHe, $^2\Sigma$ | 0.25 | 99.75 |
| $^7$LiHe, $^2\Pi$ | 11.5 | 88.5 |

[a]Results are listed for the two resonances $^2\Sigma$ and $^2\Pi$ and for the two isotopes $^6$Li and $^7$Li.

that the internuclear distance associated with the maximum value of the decay rate of $^2\Pi$ corresponds to an internuclear distance where the potential of the cation is more attractive than that for $^2\Sigma$ (see Figure 1). Nevertheless, the quantum prediction of the amount of the bound cation products formed from the $^2\Pi$ state (less than 12%) is much smaller than the prediction of the reflection principle (almost no dissociative products). These facts imply that the behavior of the ICD reaction within LiHe is not semiclassical, and we should consult quantum effects for interpreting this reaction.

The results presented in Figure 2 and Table 1 are obtained by taking $t \to \infty$ in the following exprssion[36,37]

$$\sigma^{\alpha}(E_j^{\mathrm{cat}}, t) = \int \mathrm{d}E_{\mathrm{el}} \left| \sum_{\nu} \left[ \left(\phi_j^{\mathrm{cat}} \middle| \sqrt{\frac{\Gamma^{\alpha}(R)}{2\pi}} \middle| \psi_{\nu}^{\alpha}\right)(\psi_{\nu}^{\alpha}|\phi^{\mathrm{gs}}) \frac{1 - \mathrm{e}^{\mathrm{i}(E_j^{\mathrm{cat}} + E_{\mathrm{el}} - E_{\nu}^{\alpha})t/\hbar}}{E_j^{\mathrm{cat}} + E_{\mathrm{el}} - E_{\nu}^{\alpha}} \right] \right|^2 \quad (1)$$

where $t$ represents the time after the excitation of the LiHe system. This expression describes the probability to obtain the $j$th nuclear state $\phi_j^{\mathrm{cat}}$ of the cationic ICD product associated with the eigenenergy $E_j^{\mathrm{cat}}$, after excitation of the neutral LiHe molecule in its ground state into the metastable $\alpha$ state (in our case, $\alpha$ can be $^2\Sigma$ or $^2\Pi$). $\Gamma^{\alpha}(R)$ is the electronic decay rate as a function of the internuclear separation of the metastable $\alpha$ state, and $\psi_{\nu}^{\alpha}$ is the $\nu$th nuclear state of the metastable $\alpha$ electronic state that corresponds to the complex eigenenergy $E_{\nu}^{\alpha}$. Because $\psi_{\nu}^{\alpha}$ is an eigenstate of a non-Hermitian Hamiltonian (with complex potential), the c-product $(\cdots|\cdots)$ is used rather the scaler product $\langle\cdots|\cdots\rangle$.[38] $E_{\mathrm{el}}$ is the kinetic energy of the emitted ICD electron, and $\phi^{\mathrm{gs}}$ is the diffuse nuclear wave function of the ground rovibrational and electronic state of the neutral LiHe calculated using the potential borrowed from ref 2. Notice that because of the complex value of $E_{\nu}^{\alpha}$, taking the limit of $t \to \infty$ in eq 1 leads to the time-independent expression

$$\sigma^{\alpha}(E_j^{\mathrm{cat}}) = \int \mathrm{d}E_{\mathrm{el}} \left| \sum_{\nu} \left[ \frac{\left(\phi_j^{\mathrm{cat}} \middle| \sqrt{\frac{\Gamma^{\alpha}(R)}{2\pi}} \middle| \psi_{\nu}^{\alpha}\right)(\psi_{\nu}^{\alpha}|\phi^{\mathrm{gs}})}{E_j^{\mathrm{cat}} + E_{\mathrm{el}} - E_{\nu}^{\alpha}} \right] \right|^2 \quad (2)$$

However, to avoid artificial reflections of the dissociative nuclei, $Li^+$ and He, from the edge of the box used in the calculations, we use eq 1 (with very large value of $t$) rather than eq 2, which are equivalent. The KER spectra in Figure 2 are obtained by calculating $\sigma^{\alpha}(E_j^{\mathrm{cat}})$ with $E_j^{\mathrm{cat}}$ values that are larger than the asymptotic energy of the cation (sum of the atomic He and $Li^+$ energies at their ground state) where the KER (kinetic energy released by the nuclei) equals the difference between $E_j^{\mathrm{cat}}$ and the asymptotic energy of the cation. Because we use box calculations which yield a discrete continuum spectrum of $E_j^{\mathrm{cat}}$, we multiply the expression in eq 1/eq 2 by the density of states $\rho$(KER) in order to get a proper continuum spectrum of the KER. The fraction of the cationic products which are bound molecules (presented in Table 1) is obtained by summing over all $\sigma^{\alpha}(E_j^{\mathrm{cat}})$ with $E_j^{\mathrm{cat}}$ that is smaller than the asymptotic energy of the cation potential and corresponds to a bound state, divided by the summation over all $\sigma^{\alpha}(E_j^{\mathrm{cat}})$.

The numerical evaluation of eq 1 was done using the one-dimensional particle in a box basis functions. The chosen parameters for which we obtained converged results and a complete description of the extended wave function of the ground rovibrational and electronic state of the neutral LiHe are as follows: box length, $L$ = 600 a.u. = 317.5 Å; and the number of basis functions, $n$ = 6001. The smallest interatomic distance considered in the calculations is $R_{\mathrm{min}}$ = 2 a.u. = 1.06 Å. The time value employed in eq 1 is $t = 4 \times 10^5$ a.u. = 9675.5 fs for which the results have converged. Note that up to this time the wavepacket of the dissociative nuclei, $Li^+$ and He, is well located inside the box.

The peaks presented in the KER spectra (Figure 2) are results of quantum effects which have been checked for numerical convergence. To analyze these effects, we make the following simplifying approximations and concentrate on the isotope $^7$LiHe. The solid lines in Figure 3 depict the overlap

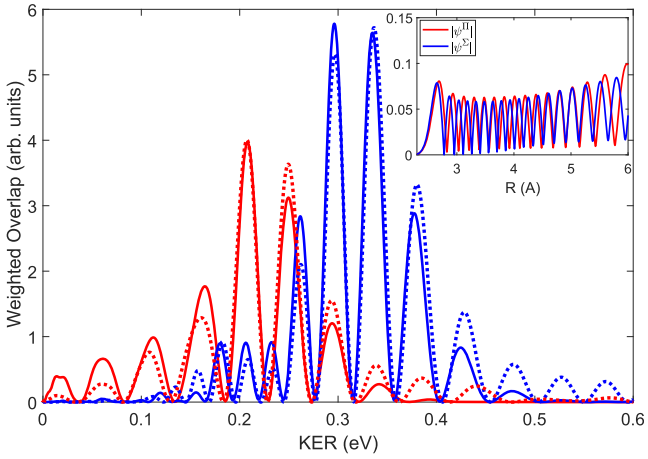


**Figure 3.** On the interpretation of the numerically exact KER spectra shown in Figure 2 for $^7$Li−He*. Shown is the weighted overlap $\left|\left(\phi_j^{\mathrm{cat}} \middle| \sqrt{\frac{\Gamma^{\Sigma/\Pi}(R)}{2\pi}} \middle| \psi^{\Sigma/\Pi}\right)\right|^2$ as a function of KER. This quantity is a dominant constituent in the expression of the KER spectrum in eq 1/eq 2. Depicted are results for two cases of $\psi^{\Sigma/\Pi}$: the most populated state of the $^2\Sigma$ (blue lines) and $^2\Pi$ (red lines) decaying states. The first case is when $\psi^{\Sigma/\Pi}$ is the numerically exact wave function (solid lines). The second case (dashed lines) is when $\psi^{\Sigma/\Pi}$ is approximated by a linear combination of Dirac delta functions, $\sum_i \psi^{\Sigma/\Pi}(R_i)\delta(R_i)$ where $R_i$ are the extrema of the numerically exact $|\psi^{\Sigma/\Pi}|$. As an example we show the numerically exact $|\psi^{\Sigma}|$ and $|\psi^{\Pi}|$ in the inset. The agreement between the two cases demonstrates that the phase shifts between the cationic and the resonance wave functions determine the peaks in the KER spectra and explain the oscillatory behavior of the spectra (see text for details).



https://dx.doi.org/10.1021/acs.jpclett.0c01974
J. Phys. Chem. Lett. 2020, 11, 6600−6605

between the final states and the resonance state weighted by the coupling to the ionization continuum (square root of the decay rate) $\left|\left(\phi_j^{\text{cat}}\left|\sqrt{\frac{\Gamma^{\Sigma/\Pi}(R)}{2\pi}}\right|\psi^{\Sigma/\Pi}\right)\right|^2$ as a function of KER, where $\psi^{\Sigma/\Pi}$ represents the most populated vibrational state of the $^2\Sigma$ or the $^2\Pi$ electronic states. This weighted overlap is a dominant constituent in the expression of the KER spectrum in eq 1/eq 2. As can be seen from the comparison of Figures 2 and 3, this expression is responsible for the peaks appearing in the KER spectra. To interpret these peaks we approximate the resonance nuclear wave function $\psi^{\Sigma/\Pi}$ in the weighted overlap. The vibrational resonance wave function $\psi^{\Sigma/\Pi}$ is highly oscillatory (see inset in Figure 3), and we approximate it by a linear combination of delta peaks $\psi^{\Sigma/\Pi} = \sum_i \psi^{\Sigma/\Pi}(R_i)\delta(R_i)$, where $R_i$ are the positions of the extrema of the numerically exact $|\psi^{\Sigma/\Pi}|$ and $\delta(R_i)$ are Dirac delta functions. With this approximation, the expression for the weighted overlap simplifies, yielding

$$\left|\left(\phi_j^{\text{cat}}\left|\sqrt{\frac{\Gamma^{\Sigma/\Pi}(R)}{2\pi}}\right|\psi^{\Sigma/\Pi}\right)\right|^2 \approx \left|\sum_i\left[\phi_j^{\text{cat}}(R_i)\sqrt{\frac{\Gamma^{\Sigma/\Pi}(R_i)}{2\pi}}\psi^{\Sigma/\Pi}(R_i)\right]\right|^2 \quad (3)$$

The dashed lines in Figure 3 show the result of eq 3 as a function of the KER. Clearly, eq 3 recovers well the peaks obtained by the numerically exact weighted overlap (solid lines in Figure 3). Thus, the approximate expression in eq 3 explains the appearance of peaks and also of the dips in the KER spectra. A dip is obtained when the cation wave function $\phi_j^{\text{cat}}$ exhibits a node at an extremum of the resonance wave function, while a peak observed whenever the cation wave function $\phi_j^{\text{cat}}$ has an extremum at the same interatomic distance as the resonance wave function. This leads to the interpretation of the KER spectra associated with the phase shift between the cationic and the resonance wave functions; a peak is obtained for $n\pi$ phase shift while a dip for a phase shift of $(2n + 1)\pi/2$, where $n$ is an integer.

Apart from having led to the interpretation of the peaks in the KER spectra, eq 3 also demonstrates that the dissociative nuclear wave functions of the cation must be considered in order to understand the ICD reaction in LiHe. As we have seen, the quantum property of these wave functions responsible for the behavior of the KER spectra is their phase shift relative to the resonance wave functions. The semiclassical reflection principle, which precisely explained ICD in the helium dimer,[20] does not account for the quantum behavior of the cationic states and therefore fails in interpreting ICD in LiHe.

To round out the discussion, we further simplify eq 3 by expressing the dissociative nuclear wave function of the cation by a transparent analytic approximation which explicitly reflects the nature of oscillations of this function. At each KER, the respective dissociative wave function is related to an inner classical turning point which is determined by the repulsive part of the cationic potential (see Figure 1). As this point is far outside the range of the vibrational resonance states, we approximately set there the cationic function to zero as if it was a true turning point and neglect the influence of the potential well on the wave function. Consequently, a cation dissociative nuclear wave function $\phi_j^{\text{cat}}(R)$ is approximated to behave as $\sin(\sqrt{2\mu E_j^{\text{KER}}}(R - R_{E_j^{\text{KER}}}))$. $E_j^{\text{KER}}$ is the KER associated with this wave function; $R_{E_j^{\text{KER}}}$ is the inner classical turning point of this wave function, and $\mu$ is the reduced mass of LiHe. Notice however, that using this assumption does not recover the exact positions of the peaks in the KER spectra (Figure 4). The reason for that is the inaccurate

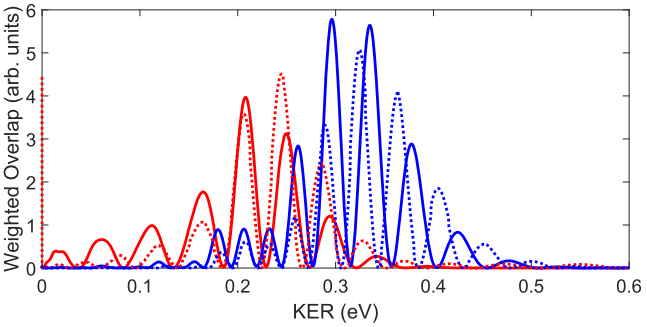


**Figure 4.** Interpretation of the numerically exact KER spectra shown in Figure 2 for $^7$Li−He* employing the simplified expressions in eq 4. As in Figure 3, the weighted overlaps for the $^2\Sigma$ and the $^2\Pi$ resonances computed numerically using exact wave functions are shown as red and blue solid lines, respectively. The respective results obtained using the simplified expressions in eq 4 are shown as dashed lines. The underlying approximate wave functions with their classical turning point cannot recover the exact positions of the peaks (see text). Nevertheless, the sinusoidal approximation for the cationic dissociative wave functions applied in eq 4 does provide a semiquantitative explanation for the source of the peaks and the oscillatory behavior of the KER spectra.

approximation, in which we assign a zero value to $\phi_j^{\text{cat}}(R)$ at its classical turning point. Adjusting $R_{E_j^{\text{KER}}}$ in order to patch these KER spectra is equivalent to adding an energy-dependent phase to the sine functions. However, in order to provide a semiquantitative explanation for the source of the peaks, it is sufficient to use sinusoidal approximation for the cationic wave function with an arbitrary phase. Substituting this sinusoidal shape of the dissociative nuclear wave functions into eq 3 yields the explicit expression

$$\left|\sum_i\left[\psi^{\Sigma/\Pi}(R_i)\sqrt{\frac{\Gamma^{\Sigma/\Pi}(R_i)}{2\pi}} \times \sin(\sqrt{2\mu E_j^{\text{KER}}}(R_i - R_{E_j^{\text{KER}}}))\right]\right|^2 \quad (4)$$

which oscillates with the KER. The dashed lines in Figure 4 show the result of eq 4 as a function of the KER, while the solid lines in Figure 4 show the numerically exact weighted overlap. The exact dissociative wave functions are indeed found to be sinusoidal in the $R$ range of the vibrational resonances, and eq 4 can be seen as an explanation of the oscillatory behavior of the KER spectra.

To conclude, the ICD reaction within the extreme LiHe dimer is controlled by quantum effects. By performing accurate nuclear calculations we have determined the KER spectra and


https://dx.doi.org/10.1021/acs.jpclett.0c01974
J. Phys. Chem. Lett. 2020, 11, 6600−6605

the fraction of the bound and dissociative products of the ICD process within LiHe. Interestingly, the latter products dominate by far. The semiclassical reflection principle, which was highly successfully used for ICD in $He_2$, fails in predicting these results, although LiHe shares many properties with $He_2$ (very extended ground-state wave functions, very large average internuclear distances, and tiny binding energies). Applying the semiclassical reflection principle does not require knowledge of the dissociative wave function. In complete contrast, the understanding of the KER in LiHe requires detailed knowledge of this function. Specifically, the phase shift between the nuclear wave functions of the decaying species and the cationic product determines the structure of the KER spectra for ICD in LiHe. The different character of the ICD reaction of LiHe and $He_2$ can be associated with the strength of the electrostatic repulsion between the two nuclei of the ICD product. In the $He_2$ case, the final ICD state undergoes Coulombic explosion due to the strong electrostatic repulsion between the two charged nuclei ($He^+ + He^+$), whereas in the product of the LiHe ICD, the electrostatic repulsion is weak at the distances where the ICD reaction occurs. In summary, we find the ICD in LiHe to be an intriguing process which calls for experiments.

## AUTHOR INFORMATION


### Corresponding Author

**Nimrod Moiseyev** − *Schulich Faculty of Chemistry, Technion-Israel Institute of Technology, Haifa 32000, Israel;* Email: nimrod@technion.ac.il

### Authors

**Anael Ben-Asher** − *Schulich Faculty of Chemistry, Technion-Israel Institute of Technology, Haifa 32000, Israel;* orcid.org/0000-0002-9174-8801

**Arie Landau** − *Schulich Faculty of Chemistry, Technion-Israel Institute of Technology, Haifa 32000, Israel; Theoretische Chemie, Physikalisch-Chemisches Institut, Universität Heidelberg, Heidelberg D-69120, Germany;* orcid.org/0000-0002-1924-1555

**Lorenz S. Cederbaum** − *Theoretische Chemie, Physikalisch-Chemisches Institut, Universität Heidelberg, Heidelberg D-69120, Germany;* orcid.org/0000-0002-4598-0650

Complete contact information is available at: https://pubs.acs.org/10.1021/acs.jpclett.0c01974


### Notes

The authors declare no competing financial interest.

## ACKNOWLEDGMENTS

This research was supported by the Israel Science Foundation (Grant No. 1661/19). L.S.C. gratefully acknowledges funding from the European Research Council (Advanced Investigator Grant No. 692657). A.B.A. gratefully acknowledges the support of the Adams Fellowship Program of the Israel Academy of Sciences and Humanities.

## REFERENCES


(1) Tariq, N.; Taisan, N. A.; Singh, V.; Weinstein, J. D. Spectroscopic Detection of the LiHe Molecule. *Phys. Rev. Lett.* **2013**, *110*, 153201.

(2) Kleinekathöfer, U.; Lewerenz, M.; Mladenović, M. Long Range Binding in Alkali-Helium Pairs. *Phys. Rev. Lett.* **1999**, *83*, 4717−4720.

(3) Friedrich, B. A Fragile Union Between Li and He Atoms. *Physics* **2013**, *6*, 42.

(4) Jensen, A.; Riisager, K.; Fedorov, D. V.; Garrido, E. Structure and Reactions of Quantum Halos. *Rev. Mod. Phys.* **2004**, *76*, 215−261.

(5) Cederbaum, L.; Zobeley, J.; Tarantelli, F. Giant Intermolecular Decay and Fragmentation of Clusters. *Phys. Rev. Lett.* **1997**, *79*, 4778−4781.

(6) Scheit, S.; Averbukh, V.; Meyer, H.-D.; Moiseyev, N.; Santra, R.; Sommerfeld, T.; Zobeley, J.; Cederbaum, L. On the Interatomic Coulombic Decay in the Ne Dimer. *J. Chem. Phys.* **2004**, *121*, 8393−8398.

(7) Morishita, Y.; Liu, X.-J.; Saito, N.; Lischke, T.; Kato, M.; Prümper, G.; Oura, M.; Yamaoka, H.; Tamenori, Y.; Suzuki, I.; et al. Experimental Evidence of Interatomic Coulombic Decay from the Auger Final States in Argon Dimers. *Phys. Rev. Lett.* **2006**, *96*, 243402.

(8) Jahnke, T.; Sann, H.; Havermeier, T.; Kreidi, K.; Stuck, C.; Meckel, M.; Schöffler, M.; Neumann, N.; Wallauer, R.; Voss, S.; et al. Ultrafast Energy Transfer Between Water Molecules. *Nat. Phys.* **2010**, *6*, 139−142.

(9) Takanashi, T.; Golubev, N.; Callegari, C.; Fukuzawa, H.; Motomura, K.; Iablonskyi, D.; Kumagai, Y.; Mondal, S.; Tachibana, T.; Nagaya, K.; et al. Time-Resolved Measurement of Interatomic Coulombic Decay Induced by Two-Photon Double Excitation of $Ne_2$. *Phys. Rev. Lett.* **2017**, *118*, No. 033202.

(10) Ren, X.; Miteva, T.; Kolorenč, P.; Gokhberg, K.; Kuleff, A. I.; Cederbaum, L. S.; Dorn, A. Observation of Fast and Slow Interatomic Coulombic Decay in Argon Dimers Induced by Electron-Impact Ionization. *Phys. Rev. A: At., Mol., Opt. Phys.* **2017**, *96*, No. 032715.

(11) Santra, R.; Zobeley, J.; Cederbaum, L. S.; Moiseyev, N. Interatomic Coulombic Decay in Van der Waals Clusters and Impact of Nuclear Motion. *Phys. Rev. Lett.* **2000**, *85*, 4490−4493.

(12) Marburger, S.; Kugeler, O.; Hergenhahn, U.; Möller, T. Experimental Evidence for Interatomic Coulombic Decay in Ne Clusters. *Phys. Rev. Lett.* **2003**, *90*, 203401.

(13) Nagaya, K.; Iablonskyi, D.; Golubev, N.; Matsunami, K.; Fukuzawa, H.; Motomura, K.; Nishiyama, T.; Sakai, T.; Tachibana, T.; Mondal, S.; et al. Interatomic Coulombic Decay Cascades in Multiply Excited Neon Clusters. *Nat. Commun.* **2016**, *7*, 13477.

(14) Hans, A.; Küstner-Wetekam, C.; Schmidt, P.; Ozga, C.; Holzapfel, X.; Otto, H.; Zindel, C.; Richter, C.; Cederbaum, L. S.; Ehresmann, A.; et al. Core-level Interatomic Coulombic Decay in Van der Waals Clusters. *Phys. Rev. Res.* **2020**, *2*, No. 012022.

(15) Mucke, M.; Braune, M.; Barth, S.; Förstel, M.; Lischke, T.; Ulrich, V.; Arion, T.; Becker, U.; Bradshaw, A.; Hergenhahn, U. A Hitherto Unrecognized Source of Low-Energy Electrons in Water. *Nat. Phys.* **2010**, *6*, 143−146.

(16) Stoychev, S. D.; Kuleff, A. I.; Cederbaum, L. S. Intermolecular Coulombic Decay in Small Biochemically Relevant Hydrogen-Bonded Systems. *J. Am. Chem. Soc.* **2011**, *133*, 6817−6824.

(17) Gokhberg, K.; Kolorenč, P.; Kuleff, A. I.; Cederbaum, L. S. Site- and Energy-Selective Slow-Electron Production Through Intermolecular Coulombic Decay. *Nature* **2014**, *505*, 661−663.

(18) Trinter, F.; Schöffler, M.; Kim, H.-K.; Sturm, F.; Cole, K.; Neumann, N.; Vredenborg, A.; Williams, J.; Bocharova, I.; Guillemin, R.; et al. Resonant Auger Decay Driving Intermolecular Coulombic Decay in Molecular Dimers. *Nature* **2014**, *505*, 664−666.

(19) Havermeier, T.; Jahnke, T.; Kreidi, K.; Wallauer, R.; Voss, S.; Schöffler, M.; Schössler, S.; Foucar, L.; Neumann, N.; Titze, J.; et al. Interatomic Coulombic Decay Following Photoionization of the Helium Dimer: Observation of Vibrational Structure. *Phys. Rev. Lett.* **2010**, *104*, 133401.

(20) Sisourat, N.; Kryzhevoi, N. V.; Kolorenč, P.; Scheit, S.; Jahnke, T.; Cederbaum, L. S. Ultralong-Range Energy Transfer by Interatomic Coulombic Decay in an Extreme Quantum System. *Nat. Phys.* **2010**, *6*, 508−511.

(21) Luo, F.; McBane, G. C.; Kim, G.; Giese, C. F.; Gentry, W. R. The Weakest Bond: Experimental Observation of Helium Dimer. *J. Chem. Phys.* **1993**, *98*, 3564−3567.

(22) Grisenti, R.; Schöllkopf, W.; Toennies, J.; Hegerfeldt, G.; Köhler, T.; Stoll, M. Determination of the Bond Length and Binding




https://dx.doi.org/10.1021/acs.jpclett.0c01974
J. Phys. Chem. Lett. 2020, 11, 6600−6605

Energy of the Helium Dimer by Diffraction from a Transmission Grating. *Phys. Rev. Lett.* **2000**, *85*, 2284−2287.
(23) Moiseyev, N.; Santra, R.; Zobeley, J.; Cederbaum, L. S. Fingerprints of the Nodal Structure of Autoionizing Vibrational Wave Functions in Clusters: Interatomic Coulombic Decay in Ne Dimer. *J. Chem. Phys.* **2001**, *114*, 7351−7360.
(24) Weber, T.; Czasch, A. O.; Jagutzki, O.; Müller, A.; Mergel, V.; Kheifets, A.; Rotenberg, E.; Meigs, G.; Prior, M. H.; Daveau, S.; et al. Complete Photo-Fragmentation of the Deuterium Molecule. *Nature* **2004**, *431*, 437−440.
(25) Landau, A.; Ben-Asher, A.; Gokhberg, K.; Cederbaum, L. S.; Moiseyev, N. Ab Initio Complex Potential Energy Curves of the He*(1s2p $^1$P)−Li Dimer. *J. Chem. Phys.* **2020**, *152*, 184303.
(26) Ben Ltaief, L.; Shcherbinin, M.; Mandal, S.; Krishnan, S.; LaForge, A.; Richter, R.; Turchini, S.; Zema, N.; Pfeifer, T.; Fasshauer, E.; et al. Charge Exchange Dominates Long-Range Interatomic Coulombic Decay of Excited Metal-Doped Helium Nanodroplets. *J. Phys. Chem. Lett.* **2019**, *10*, 6904−6909.
(27) Landau, A.; Bhattacharya, D.; Haritan, I.; Ben-Asher, A.; Moiseyev, N. *Adv. Quantum Chem.*; Elsevier, 2017; Vol. *74*, pp 321−346.
(28) Landau, A.; Haritan, I.; Kaprálová-Ždánská, P. R.; Moiseyev, N. Atomic and Molecular Complex Resonances from Real Eigenvalues Using Standard (Hermitian) Electronic Structure Calculations. *J. Phys. Chem. A* **2016**, *120*, 3098−3108.
(29) Landau, A.; Haritan, I. The Clusterization Technique: A Systematic Search for the Resonance Energies Obtained via Padé. *J. Phys. Chem. A* **2019**, *123*, 5091−5105.
(30) Krylov, A. I. Equation-of-Motion Coupled-Cluster Methods for Open-Shell and Electronically Excited Species: The Hitchhiker's Guide to Fock Space. *Annu. Rev. Phys. Chem.* **2008**, *59*, 433−462.
(31) Hazi, A. U.; Taylor, H. S. Stabilization Method of Calculating Resonance Energies: Model Problem. *Phys. Rev. A: At., Mol., Opt. Phys.* **1970**, *1*, 1109−1120.
(32) Landau, A. Shaping and Controlling Stabilisation Graphs for Calculating Stable Complex Resonance Energies. *Mol. Phys.* **2019**, *117*, 2029−2042.
(33) Gokhberg, K.; Kopelke, S.; Kryzhevoi, N.; Kolorenč, P.; Cederbaum, L. Dependence of Interatomic Decay Widths on the Symmetry of the Decaying State: Analytical Expressions and Ab Initio Results. *Phys. Rev. A: At., Mol., Opt. Phys.* **2010**, *81*, No. 013417.
(34) Bhattacharya, D.; Ben-Asher, A.; Haritan, I.; Pawlak, M.; Landau, A.; Moiseyev, N. Polyatomic Ab Initio Complex Potential Energy Surfaces: Illustration of Ultracold Collisions. *J. Chem. Theory Comput.* **2017**, *13*, 1682−1690.
(35) Bhattacharya, D.; Pawlak, M.; Ben-Asher, A.; Landau, A.; Haritan, I.; Narevicius, E.; Moiseyev, N. Quantum Effects in Cold Molecular Collisions from Spatial Polarization of Electronic Wave Function. *J. Phys. Chem. Lett.* **2019**, *10*, 855−863.
(36) Moiseyev, N.; Scheit, S.; Cederbaum, L. S. Non-Hermitian Quantum Mechanics: Wave Packet Propagation on Autoionizing Potential Energy Surfaces. *J. Chem. Phys.* **2004**, *121*, 722−725.
(37) Ben-Asher, A.; Moiseyev, N. The Boomerang Effect in Electron-Hydrogen Molecule Scattering as Determined by Time-Dependent Calculations. *J. Chem. Phys.* **2017**, *146*, 204303.
(38) Moiseyev, N. *Non-Hermitian Quantum Mechanics*; Cambridge University Press: Cambridge, 2011.


https://dx.doi.org/10.1021/acs.jpclett.0c01974
*J. Phys. Chem. Lett.* 2020, 11, 6600−6605